were made with respect to Al: Kelly's[16] 22- and 33-MeV α bombardment of Cu gives results that are higher than ours for 5.5- and 8-MeV protons by 0.9 and 1.3%, respectively. Heller[17] used 7.9-MeV deuterons in Ni and Cu. The Ni results are higher than ours by 1.4%, the Cu results lower by 0.4%. Wilson[18] bombarded Fe, Ni, Cu, and Zn with 4-MeV protons. His data are lower than ours by 0.5, 4.6, 3.8, and 3.4%, respectively. Teasdale's[19] 12-MeV proton measurements are lower by 0.2% for Ni, and higher by 0.8% for Cu, than ours.

It is concluded that there are no significant disagreements between our results and the quoted experiments. Although most of the quoted results are considerably less accurate than ours, it is worth noting that there is no over-all systematic deviation between our data and the quoted ones.

For the tables the agreement is usually quite good for well-known elements, while disagreements exist for elements where experimental data are scarce.

A detailed discussion will be given in a following paper,[6] where our results are used for the evaluation of shell corrections and of mean excitation potentials.

[16] E. L. Kelly, Phys. Rev. **75**, 1006 (1949).
[17] Z. H. Heller and D. J. Tendam, Phys. Rev. **84**, 905 (1951).
[18] R. R. Wilson, Phys. Rev. **60**, 749 (1941).
[19] J. G. Teasdale, University of California, Los Angeles, Report No. NP-1368, 1949 (unpublished).

ACKNOWLEDGMENTS

We want to thank the Niels Bohr Institute of the University of Copenhagen for giving us the opportunity to use their tandem Van de Graaff accelerator. The excellent technical assistance of B. Bordrup, G. Dalsgaard, and A. Nordskov Nielsen is greatly appreciated. The continuous interest of Professor O. Kofoed-Hansen and Professor J. Lindhard is gratefully acknowledged.

PHYSICAL REVIEW VOLUME 175, NUMBER 2 10 NOVEMBER 1968

Electron-Nuclear Double Resonance of the Self-Trapped Hole in LiF* †

RAMAYANA GAZZINELLI
Instituo Central de Fisica, Universidade Federal de Minas Gerais, Belo Horizonte, Brazil
AND
ROBERT LEE MIEHER‡
Department of Physics, Purdue University, Lafayette, Indiana
(Received 18 March 1968)

An electron-nuclear double-resonance (ENDOR) study of the self-trapped hole in LiF is reported. The results agree with the accepted model, i.e., the hole is shared by two halide-ion lattice sites in the form of a negatively charged diatomic halide molecule (F_2^- in this study). The variations in the ENDOR spectra for different ESR lines is investigated theoretically and experimentally. The observation of negative-contact hyperfine constants for most ENDOR nuclei is explained by exchange polarization of the "closed-shell" molecular orbitals.

I. INTRODUCTION

THE self-trapped hole or V_K center was discovered by Känzig[1] in an electron-spin-resonance (ESR) study of KCl exposed to x rays at liquid-nitrogen temperatures. Castner and Känzig[2] carried out an ESR investigation of the V_K center in several alkali halides. These ESR studies showed the V_K center to be a negatively charged diatomic halide molecule (e.g., F_2^-) with the molecular axis oriented in a [110] crystal direction. Also, there was strong indirect evidence that the molecule was located on two halide-ion lattice sites, and that the center was not associated with any other lattice defects such as impurities or vacancies. An excellent introduction to the ESR of the V_K center has been given by Slichter.[3]

Castner and Känzig tentatively correlated the V_K center with the V_1 optical band. However, Delbecq, Smaller, and Yuster[4] showed that the defect was

* Work supported by the National Science Foundation under Grant Nos. NSF-GP-53 and NSF-GP-3385 at Columbia and No. NSF-GP-4860 at Purdue.
† Partially based upon a thesis submitted by R. Gazzinelli for the Ph.D. degree at Columbia University.
‡ Alfred P. Sloan Foundation Fellow.
[1] W. Känzig, Phys. Rev. **99**, 1890 (1955).
[2] T. G. Castner and W. Känzig, J. Phys. Chem. Solids **3**, 178 (1957).
[3] C. P. Slichter, *Principles of Magnetic Resonance* (Harper and Row, New York, 1963).
[4] C. J. Delbecq, B. Smaller, and P. H. Yuster, Phys. Rev. **111**, 1235 (1958).

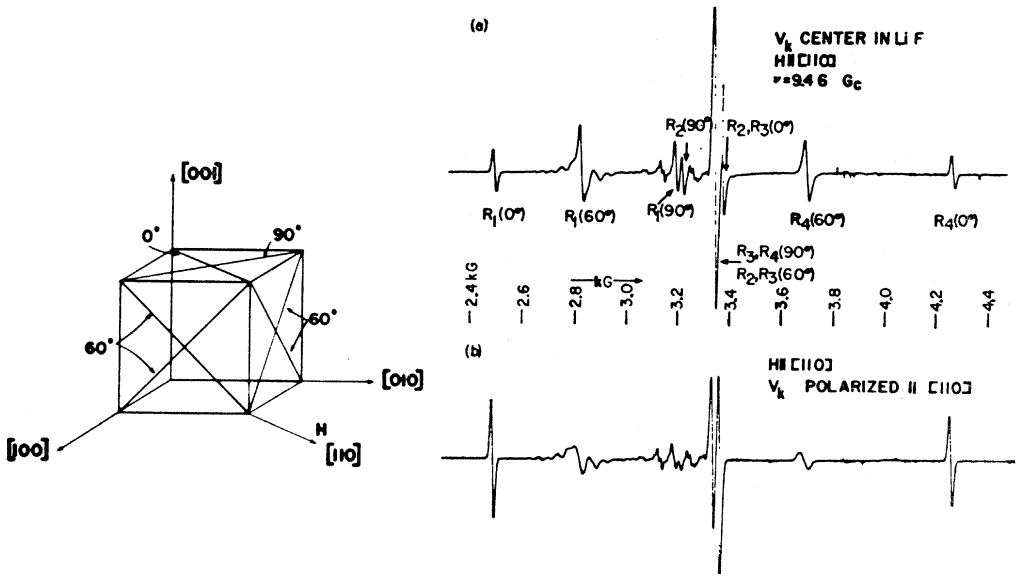

FIG. 1. The ESR spectra of V_K center in LiF for $H_0 \parallel [110]$. (a) V_K centers distributed on six possible orientations, (b) V_K centers oriented to a high degree along [110]. The spectrum of another paramagnetic center, due to the doping, appears. One sharp line in the center is due to x irradiation of the quartz finger.

responsible for an optical absorption band on the short-wavelength side of the V_1 band, and another in the infrared. The band in the ultraviolet had been previously ignored because it is almost completely covered by the V_1 band, while the band in the infrared has a very weak oscillator strength. They also made polarization studies that agreed with the orientation for the V_K center assigned by Castner and Känzig. The optical studies were extended to other alkali halides by Delbecq, Hayes, and Yuster.[5]

This article presents the results of an electron-nuclear double-resonance (ENDOR) study of the V_K center[6] in LiF which verifies the molecule ion model and yields additional information on the wave function of the unpaired spin. We shall now review the ESR and optical studies of the V_K center in LiF which are important for an understanding of the present investigation.

A. ESR Spectrum

Woodruff and Känzig[7] made a detailed ESR study of the V_K center in LiF, and the reader is referred to their article for additional details of the ESR spectrum. If the dc magnetic field H_0 is applied in an arbitrary direction, there are six possible orientations of the V_K center. Therefore, the ESR spectrum is the superposition of six spectra. Each set is characterized by the angle ζ between H_0 and the axis through the two nuclei of the molecule. For certain directions of H_0, however, some sets become equivalent, and the situation is simplified considerably. For instance, for H_0 parallel to [110] there are only three nonequivalent orientations for the F_2^- molecular ion: of the six sets, four become equivalent with $\zeta=60°$, another has $\zeta=90°$, and the remaining set has $\zeta=0°$. Figure 1 illustrates this.

Let us now fix our attention on a particular set of V_K centers. The hole is shared equally by two fluorine ions and interacts strongly with the magnetic moments of the two nuclei, resulting in a resolved hyperfine structure. There are two spin states for each of the fluorine nuclei, and therefore the ESR spectrum will consist of four lines. Following the notation of Woodruff and Känzig, we call these lines R_1, R_2, R_3, and R_4 corresponding respectively to $M=+1$, 0, 0, and -1; $M=m_1+m_2$ is the nuclear spin state of the molecular ion. The two center lines R_2 and R_3 are separate only when the angle ζ is near 90°, because of second-order effects.

It was found that the ESR spectrum of the V_K center in LiF is axially symmetric (although the center has orthorhombic symmetry) and that the position of hyperfine structure lines is a function only of ζ. A graph showing the angular dependence of the ESR spectrum, reproduced from the article by Woodruff and Känzig, is shown in Fig. 2. The g shift was found to be very small, indicating a strong quenching of angular momentum. The value was positive, as expected for a hole center.

Portis[8] has shown that the saturation behavior of

[5] C. J. Delbecq, W. Hayes, and P. H. Yuster, Phys. Rev. **121**, 1043 (1961).
[6] R. Gazzinelli and R. Mieher, Phys. Rev. Letters **12**, 644 (1964).
[7] T. O. Woodruff and W. Känzig, J. Phys. Chem. Solids **9**, 70 (1958).
[8] A. M. Portis, Phys. Rev. **91**, 1071 (1953).

ESR lines depends on the line-broadening mechanism. He distinguished between homogeneous broadening and inhomogeneous broadening. Homogeneous broadening occurs when the energy absorbed from the microwave field is distributed to all spins, and thermal equilibrium is maintained in the spin system during resonance. It may arise, for instance, from dipolar interactions between like spins. In the case of inhomogeneous broadening, the energy is transferred only to those spins whose local fields satisfy the resonance condition. The unpaired electron of a paramagnetic center may have comparable hyperfine interaction with several neighboring lattice nuclei; then the energy levels of a given electron depend on the orientation of the spins of nearby nuclei. The set of all electron spins which have the same magnetic environment constitutes a "spin packet." The large number of different spin arrangements produces a multitude of overlapping lines that appear in ESR as an inhomogeneous broadened line. Inhomogeneous broadening is a quite common phenomenon, and sometimes even very narrow lines may show this broadening.

Castner[9] studied in detail the saturation of the resonance of the V_K center. From the saturation behavior and the line shape he concluded that the lines were inhomogeneously broadened by the hyperfine interaction with surrounding lattice nuclei. He also showed that the saturation behavior was dependent in a complex way on the angle ζ and on the hyperfine structure line which was being observed. Values of the spin-lattice relaxation time T_1 and spin dephasing time T_2 were determined.

B. Optical Properties

Delbecq, Hayes, and Yuster[5] made a detailed optical study of the V_K center in LiF. They found two absorption bands due to the imperfection, at 348 and 750 mμ.

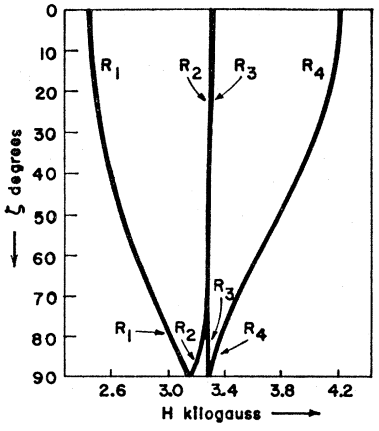

FIG. 2. Angular dependence of the ESR spectrum of V_K center in LiF for a microwave frequency of 9.3 Gc/sec. ζ is the angle between the axis of the center and the dc magnetic field H_0. Based on Woodruff and Känzig (Ref. 7).

[9] T. G. Castner, Phys. Rev. **115**, 1506 (1959).

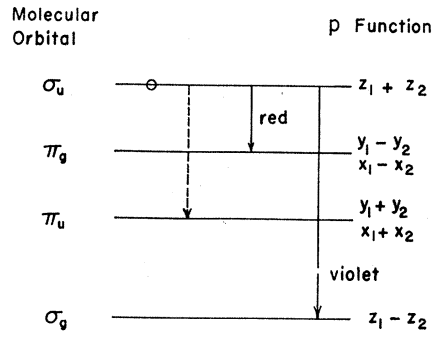

FIG. 3. Energy-levels scheme of the F_2^- molecular ion (schematic). Full arrows represent allowed optical transitions; broken arrows represent the transitions that produce the g shift.

The ultraviolet band has strong oscillator strength and corresponds to a completely anisotropic linear oscillator along the axis of the molecule. The infrared band with very small oscillator strength is partially anisotropic, corresponding to an incompletely anisotropic oscillator on the plane perpendicular to the axis of the molecule. This partial isotropy may result from a degeneracy of levels such that the transition is a superposition of different types of transitions.

Therefore, to bleach a particular set of V_K centers one irradiates the crystal with light in the 348-mμ region polarized with the electric vector parallel to the axis of the center in question. A small number of centers will be destroyed, but the large majority will reorient on the other possible orientations. By repeating the operation for different sets one may reorient the centers in a single direction. A more efficient technique to reduce the six sets of V_K centers to one set is to irradiate the crystal with unpolarized light in the 348-mμ region so that the propagation direction is parallel to the axis of the set whose population one wants to increase. Figure 1 shows two ESR spectra for H_0 parallel to [110]; (a) refers to an unpolarized sample, and (b) is the same sample after the V_K centers were reoriented on the [110] direction. The gains are the same for both runs. One observes that the 0° spectrum increased while the 60° and 90° spectra decreased.

The optical properties of the V_K center were successfully explained by a molecular orbital scheme.[5,10,11] Consider an F_2^- molecule with axis Z. There are eleven $2p$ electrons to fill the levels σ_g, π_u, π_g, and σ_u (Fig. 3). Each of the levels π_u and π_g are doubly degenerate in free space, but in the crystal the degeneracy is removed because of the orthorhombic symmetry. It is assumed that the ground state is $\sigma_g^2\pi_u^4\pi_g^4\sigma_u^1(^2\Sigma_u)$, i.e., the hole occupies the antibonding orbital σ_u. Das, Jette, and Knox[12] have calculated the total energy of an F_2^-

[10] M. H. Cohen, Phys. Rev. **101**, 1432 (1956).
[11] T. Inui, S. Harasawa, and Y. Obata, J. Phys. Soc. Japan **11**, 612 (1956).
[12] T. P. Das, A. N. Jette, and R. S. Knox, Phys. Rev. **134**, A1079 (1964); and (private communication).

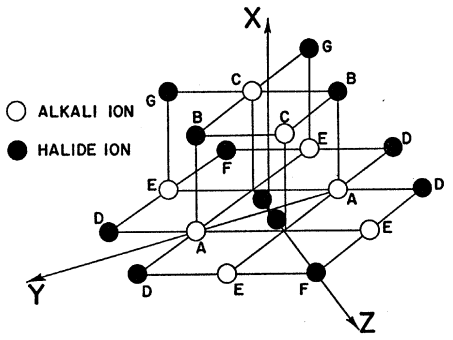

FIG. 4. V_K center in LiF lattice. X, Y, and Z are the symmetry axes of the center. The hyperfine interaction of the hole with ions A to G is resolved by ENDOR.

molecule in the lattice as a function of the molecular bond length for Σ_g and Σ_u states. They found that only the Σ_u state exhibits a minimum, providing therefore a theoretical basis for the assumption.

The band in the ultraviolet corresponds to the transition $^2\Sigma_u \rightarrow {}^2\Sigma_g$ and the band in the infrared to $^2\Sigma_u \rightarrow {}^2\Pi_g$. The transition $^2\Sigma_u \rightarrow {}^2\Pi_u$ is responsible for the g shift in the ESR spectrum, but is forbidden for electric dipole transitions.

C. Electron-Nuclear Double Resonance

For inhomogeneously broadened lines a technique still more powerful than ESR is available for the study of a paramagnetic center. This is the ENDOR introduced by Feher.[13,14] This technique, which detects direct transitions between the nuclear hyperfine levels of neighboring ions, can resolve the hyperfine structure not resolvable by ESR.

This paper reports a study of the V_K center in LiF by ENDOR. LiF was chosen for reasons of simplicity. There is only one naturally occurring fluorine isotope, F^{19}, and it has spin $\frac{1}{2}$. Therefore, the ESR spectrum, which resolves the hyperfine interaction of the hole and two fluorines, is greatly simplified. Lithium has two isotopes, Li^7 (92.6% natural abundance) and Li^6 (7.4% natural abundance). Thus one would expect in the ENDOR spectra only very weak lines due to Li^6, if they are seen at all. Also, since the electric quadrupole moment is zero for F^{19} and very small for Li^7, no quadrupole splitting of the ENDOR lines is expected.

The results verify Castner and Känzig's model of the V_K center beyond doubt; we could not find any other model that would fit the ENDOR spectra. Figure 4 shows the surrounding ions of the V_K center for which the hyperfine interaction with the hole was observed. The hole is well localized inside the shell formed by ions A to G; the density outside this shell must be very small. Precise values of the hyperfine interaction were measured for nuclei A, B, C, D, E, and F.

II. EXPERIMENTAL

A. ENDOR Technique

The ENDOR technique[13,14] constitutes a powerful method for the study of hyperfine interactions of defects in solids. The sensitivity of ENDOR is orders of magnitude greater than the direct observation of the same number of nuclei by nuclear magnetic resonance (NMR) and in favorable cases approaches the sensitivity of ESR. ENDOR, as initially employed, consisted of observing the transient change of the ESR dispersion signal when a nuclear hyperfine transition was induced at liquid-helium temperature. Feher[15] called attention to the possibility of observing stationary ENDOR signals. Seidel[16] and Lambe *et al.*[17] studied the dynamics of the process in some detail. Stationary ENDOR was used in this research, but the dynamics of the spin systems will not be considered here.

The stationary ENDOR technique consists of the following steps. Keeping the microwave frequency constant, the magnetic field is adjusted to the center of an ESR line and maintained constant. The microwave power is set at a level high enough to saturate partially the electron transition, and the ENDOR rf oscillator is swept through the frequency region of interest. In the following section we shall describe the ENDOR spectrometer that was used in this work.

B. ENDOR Spectrometer

An ENDOR spectrometer is essentially an ESR spectrometer in which provisions are made to apply to the sample an rf magnetic field H_2 perpendicular to the dc field H_0. Therefore, we discuss first the ESR spectrometer and then show how the rf field H_2 is applied to the sample. A block diagram is shown in Fig. 5.

The X-band microwave spectrometer employs a superheterodyne scheme for high sensitivity, phase-sensitive detection, and frequency locking to the sample cavity for convenience of operation. The advantages of the superheterodyne scheme have been discussed by Feher[18] and will not be repeated here.

The signal klyston is a low-noise Varian VA-242E or V203B, powered by a Hewlett-Packard model-716 power supply. The klystron is stabilized by a model-DY 2650-A Dymec oscillator synchronizer (Osc. Sync. in Fig. 5). In this unit a sample of the signal frequency beats against harmonics of the internal rf reference produced by doubling the output of a stable crystal

[13] G. Feher, Phys. Rev. **103**, 500 (1956); **103**, 834 (1956); **114**, 1219 (1959).
[14] G. Feher and E. A. Gere, Phys. Rev. **103**, 501 (1956); **114**, 1245 (1959).
[15] G. Feher, Physica Suppl. **24**, 80 (1958).
[16] H. Seidel, Z. Physik **165**, 218 (1961); **165**, 239 (1961).
[17] J. Lambe, N. Laurance, E. C. McIrvine, and R. W. Terhune, Phys. Rev. **122**, 1161 (1961).
[18] G. Feher, Bell System Tech. J. **36**, 449 (1957).

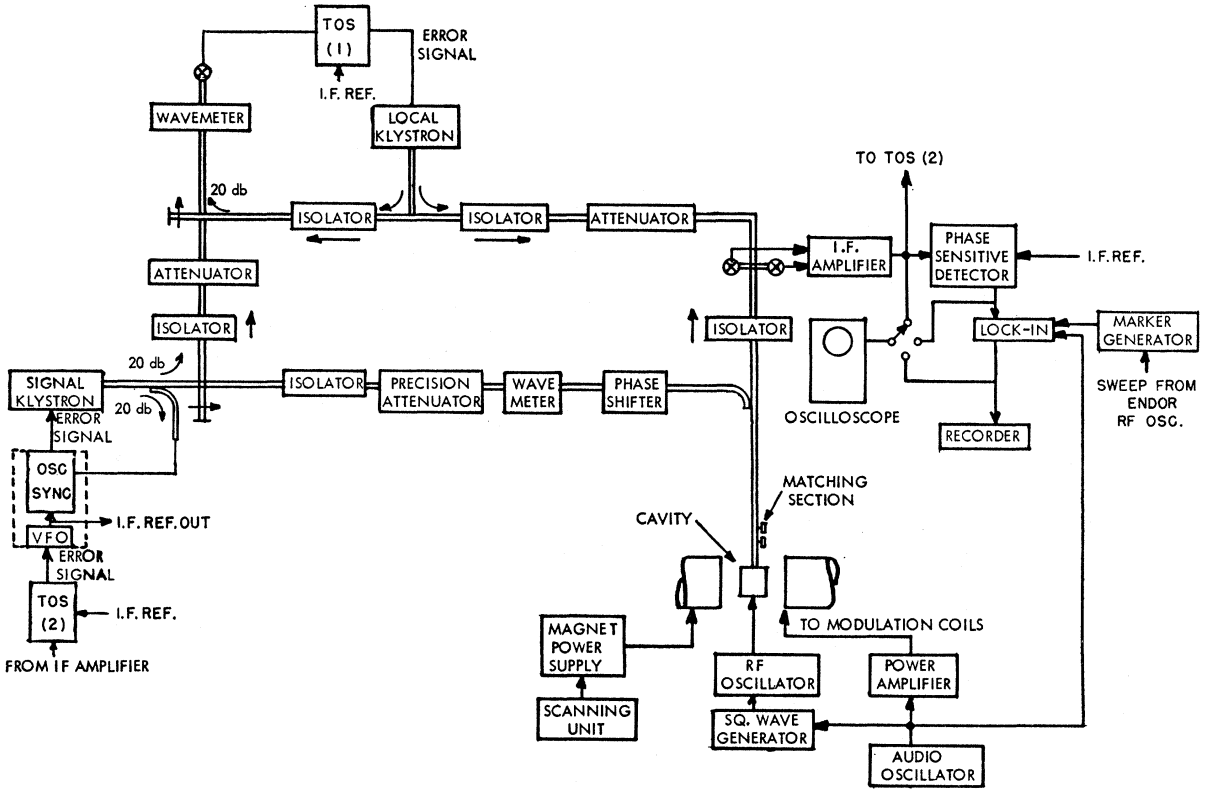

FIG. 5. Block diagram of ENDOR spectrometer.

oscillator of frequency f_0. The beat frequency, after amplification, is compared in phase with the output of the i.f. reference oscillator of variable frequency f' (29–31 Mc/sec) and the resultant phase-error voltage is added to the reflector voltage, thereby correcting any drift in phase. The signal klystron frequency is then given by $F_s = 2nf_0 \pm f'$. The frequency f' is used as the i.f. reference for all parts of the spectrometer.

The microwave power is brought to the sample cavity through an isolator, precision attenuator, wavemeter, precision phase shifter, and a directional coupler. The iris of the cavity is filled with a dielectric material chosen so that the cavity is slightly overcoupled. In the waveguide, at one wavelength distance from the iris, there is a screw that provides a fine control of the cavity match. The signal reflected from the cavity goes through an isolator to a balanced-mixer detector where it mixes with the power from the local oscillator.

The local oscillator is a low-noise reflex klystron Varian 203B, powered by a Hewlett-Packard model-716 power supply. For phase-sensitive detection the local oscillator must be locked in phase to the signal oscillator. This is done by a modified model-DY-5796 Dymec transfer oscillator synchronizer, from now on referred to as TOS (TOS No. 1 in Fig. 5). The phase comparator output terminals of this unit were insulated to receive the klystron's reflector voltage; also some filtering for 30 Mc/sec was added to these terminals to avoid any leakage of the reference rf to the klystron reflector. The local oscillator power is divided by a microwave tee. Part of it goes to the balanced detector through an isolator and an attenuator, which permits adjustment of optimum local oscillator power on the crystals. The other half is brought to a microwave diode, where it is mixed with a sample of the power from the signal klystron. The beat note is led to the TOS No. 1 where, after amplification, it is compared with the i.f. reference f'. If the local oscillator drifts in phase, an error voltage is generated and added in series to the reflector voltage. By this method the local oscillator is locked in phase with the signal klystron and tracks it with frequency $F_L = F_s \pm f'$.

There is a third loop that makes possible the locking of the signal klystron to the sample cavity. The signal from the balanced mixer is amplified by an i.f. amplifier LEL model-IF3499 (110-dB maximum gain, 30-Mc center frequency, and 2-Mc/sec bandwidth). A sample of the output is led to the TOS No. 2 where it is compared in phase with the i.f. reference f'. Any change in frequency of the cavity results in a phase change in the reflected power and an error voltage is produced by the TOS No. 2. This error voltage is led through a 0.1-sec time-constant network to the FM input of the oscillator synchronizer. This time constant was introduced so that the oscillator synchronizer responds only to the slow

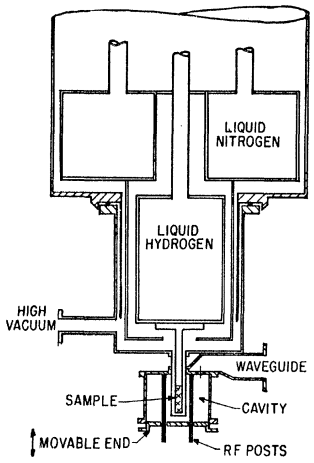

FIG. 6. Cryostat and cavity assembly (schematic).

thermal drift of the cavity. The error signal changes the i.f. frequency f' of the variable-frequency oscillator. This causes a change in the frequency of the signal klystron and the entire system tracks the cavity.

The spectrometer therefore has the advantage of very high short-term stability (one part in 10^8) and is locked to the sample cavity over a long term. Once the cavity is tuned to the frequency F_S and matched to the line, the spectrometer will operate for a long time without requiring any adjustment.

The detection is made by the usual techniques. The output of the i.f. amplifier is directed to a phase-sensitive detector designed and built in the laboratory, a lock-in amplifier (EMC model-RJB), and a recorder. The standard i.f. reference f', used throughout the spectrometer, is the reference for the demodulation after passing through an rf phase shifter. The microwave phase shifter is used only in the operation of locking the signal klystron to the cavity. The rf phase shifter is adjusted to select absorption or dispersion of the ESR.

The dc magnetic field is provided by a 6-in. Varian magnet with matching power supply. A pair of coils wound on the pole faces and driven by an audio oscillator and high-fidelity power amplifier is used for field modulation for standard ESR work.

Provisions are made to apply to the sample an rf field H_2, to induce the nuclear transitions. A scheme designed by Seidel[16] is employed in this spectrometer. The cavity is cylindrical and operates in the TE_{011} mode. (See Fig. 6.) It has a movable end (bottom) that allows tuning. To reduce thermal drift the first cavity side walls were made of quartz with deposited silver. However, after the cavity locking scheme was successful, the cavities were made of gold plated brass. The fixed end (top) has a hole in the center through which a quartz finger containing the sample extends into the cavity. For the TE_{011} mode, this is the region of maximum microwave magnetic field. The cavity is coupled to the waveguide by an iris on the fixed end.

Four thin metallic posts, parallel to the axis of the cavity, penetrate into the cavity through insulators on the bottom and are fixed on the top. They are disposed in such a way that they constitute a pair of Helmholtz coils, the sample being in the center. This arrangement is possible because in the TE_{011} mode there are no electric field lines along the posts, and therefore the Q of the cavity is not greatly decreased. The $\mathbf{H}_2$ field is approximately uniform in the region of the sample and is perpendicular to the dc magnetic field $\mathbf{H}_0$ and to microwave magnetic field $\mathbf{H}_1$.

The pair of Helmholtz coils are coupled by a loop to the tank-circuit coil of the ENDOR variable-frequency oscillator which is positioned just below the cavity. This coupling produced high rf currents in the low-impedance Helmholtz coil formed by the posts in the cavity. The tank-circuit capacitor is driven by a clock motor to sweep the frequency. Six different tank-circuit coils allow coverage of the range 0.5–70 Mc/sec.

The use of lock-in detection requires some form of modulation of the signal. Amplitude modulation of the rf has been used in this work.[16] It presents at least three advantages over magnetic field modulation: (1) there is no single resonance ESR signal to be bucked out; (2) there is no magnetic field modulation pickup; and (3) the true absorption shape of the ENDOR line is recorded. An audio oscillator that provides the reference for the lock-in amplifier, drives a square-wave modulator. The output of this modulator is applied to the cathode of the rf oscillator and turns it on and off. A 400-cps modulation frequency was used in this work.

Frequency markers on the ENDOR runs are obtained by taking a sample of the rf oscillator output to a frequency marker generator (Jerrold model-CM 10). The beat note energizes the event-marker pen of the recorder through a relay switch. Markers may be obtained at intervals of 100 kc/sec, 500 kc/sec, 1 Mc/sec, 3 Mc/sec, 5 Mc/sec, or 10 Mc/sec by selecting the appropriate oscillators on the marker generator.

C. Cryostat and X-Ray Facilities

The cryostat and cavity assembly are shown in Figure 6. The cryostat is double and allows work to be performed at liquid-nitrogen or -hydrogen temperatures. It terminates in a quartz finger that extends into the cavity. The sample inside the quartz finger is cooled by conduction. It is cemented to a piece of alkali-halide crystal and this in turn to a high-conductivity copper finger which is fixed to the bottom of the refrigerant can. Since the sample is exposed to room-temperature radiation the sample temperature is about 90°K when liquid nitrogen is in the inner can. The inner part of the cryostat can be rotated around the axis and enables one to make measurements for different orientations of the crystal with respect to $\mathbf{H}_0$.

This arrangement allows a convenient irradiation of the sample with light at low temperatures. If the cavity

is removed the crystal is protected only by the quartz finger which is transparent, from roughly 5 μ to less than 0.2 μ. This feature was extensively used in this work for polarization of the V_K center.

Facilities to irradiate the sample with x rays at low temperature were made. The cryostat is suspended from a platform which is mounted on rails on the magnet table and can be pulled out of the magnet gap for irradiation. The cavity is removed and the x-ray tube is raised so that the quartz finger enters into a hole in a lead box that is mounted on the head of the x-ray tube shield. The sample is 9 cm from the target, and there is an inherent filtration of tube and shield equivalent to 3 mm of aluminum as well as $\frac{1}{2}$ mm of quartz due to the finger. The x-ray unit is a Müller MC 150 regulated continuously in the range 50–150 kV and providing currents up to 30 mA.

D. Sample Preparation

Crystals were grown in the laboratory by the Kyropoulos method. A seed is attached to a water-cooled rod and the rod is raised at a speed of $\frac{1}{8}$ in./h. Different impurities were added to the melt to act as electron traps.

After the sample is cut (approximately 12×6×6 mm), it is quenched by heating it to about 100°C below the melting point and then placing it on a polished copper plate. A piece of pure KCl crystal is cemented to the copper finger on the cryostat, and the sample is glued to the KCl crystal. General Electric insulating varnish GE 7031 is used for this operation because of its good low-temperature properties.

The crystal is irradiated at 90°K by x rays. Voltages of 75 kV and currents of 30 mA were used. Time of irradiation varied from 7 to 15 h. An Osram Mercury lamp (model-HBO 200), a Corning Glass Filter No. 7-37, and a Glan Thompson prism were used in the orientation of the V_K centers.

Most of the results reported in this paper were obtained from LiF single crystals doped with AgF_2 (1% of the weight, added to the melt). To verify that the results were independent of the impurity added, observations were also made on LiF single crystals obtained from the Harshaw Chemical Co.

III. THEORY OF HYPERFINE STRUCTURE

Consider a paramagnetic center with electronic spin **S** and a neighboring nucleus with spin **I** in a magnetic field $\mathbf{H}_0$. The spin-Hamiltonian operator is[3,19]

$$\mathcal{H}=\gamma_e\hbar\mathbf{H}_0\cdot\mathbf{S}-\gamma_n\hbar\mathbf{H}_0\cdot\mathbf{I}+\mathcal{H}_{IS}, \tag{1}$$

where γ_e and γ_n are the gyromagnetic ratios for the electron and the nucleus, respectively. $\mathcal{H}_{IS}$ is the hyperfine-structure Hamiltonian representing the interaction between the magnetic moment of the nucleus and the electron. The interaction between the electric field gradients and the electric quadrupole moment of the nucleus is neglected because it plays no role in this investigation. The hyperfine-structure Hamiltonian is given by[3]

$$\mathcal{H}_{IS}=\gamma_e\gamma_n\hbar^2\int|\psi(r)|^2\times\left[\frac{3(\mathbf{I}\cdot\mathbf{r})(\mathbf{S}\cdot\mathbf{r})}{r^5}-\frac{\mathbf{I}\cdot\mathbf{S}}{r^3}+\tfrac{8}{3}\pi\mathbf{I}\cdot\mathbf{S}\delta(r)\right]dV, \tag{2}$$

the integration being over electron spatial coordinates. The first two terms in the integral represent the usual dipole-dipole interaction, while the third term is the contact interaction. This expression is linear in the spin variables I_x, I_y, I_z, S_x, S_y, and S_z and may be written in the form

$$\mathcal{H}_{IS}=a\mathbf{I}\cdot\mathbf{S}+\sum_{i,k=x,y,z}B_{ik}I_iS_k, \tag{3}$$

where

$$a=(8\pi/3)\gamma_e\gamma_n\hbar^2|\psi(0)|^2, \tag{4}$$

$$B_{ik}=\gamma_e\gamma_n\hbar^2\int\left[\frac{3x_ix_k}{r^5}-\frac{\delta_{ik}}{r^3}\right]|\psi(r)|^2dV. \tag{5}$$

The tensor **B** is traceless and symmetric. It is possible to make a transformation to principal axes, i.e., to diagonalize **B**. Then, representing the principal axes by x, y, and z, we obtain

$$\mathcal{H}_{IS}=a\mathbf{I}\cdot\mathbf{S}+B_xI_xS_x+B_yI_yS_y+B_zI_zS_z=\mathbf{I}\cdot\mathbf{A}\cdot\mathbf{S}, \tag{6}$$

where

$$\mathbf{A}=iA_xi+jA_yj+kA_zk \tag{7}$$

and

$$A_x=a+B_x,\qquad A_y=a+B_y,\qquad A_z=a+B_z. \tag{8}$$

From the three Eqs. (8) and the fact that **B** is traceless, one obtains immediately

$$a=\tfrac{1}{3}(A_x+A_y+A_z). \tag{9}$$

We may write the spin-Hamiltonian operator of Eq. (1) as

$$\begin{aligned}\mathcal{H}&=\gamma_e\hbar\mathbf{H}_0\cdot\mathbf{S}-\gamma_n\hbar\mathbf{H}_0\cdot\mathbf{I}+\mathbf{I}\cdot\mathbf{A}\cdot\mathbf{S}\\&=\gamma_e\hbar\mathbf{H}_0\cdot\mathbf{S}-\gamma_n\hbar\mathbf{H}_0\cdot\mathbf{I}+a\mathbf{I}\cdot\mathbf{S}\\&\quad+B_xI_xS_x+B_yI_yS_y+B_zI_zS_z.\end{aligned} \tag{10}$$

In the high-field approximation,

$$\gamma_e\hbar H_0\gg|a|,|B_x|,|B_y|,|B_z|, \tag{11}$$

the electron spin is quantized in the direction of $\mathbf{H}_0$. Let $\mathbf{H}_0$ be fixed in the system $x'y'z'$ along z', then take the eigenfunctions to be eigenfunctions of $S_{z'}$ with eigenvalues m_S. Also, if

$$|a\pm\gamma_n\hbar H_0|\gg|B_x|,|B_y|,|B_z|, \tag{12}$$

[19] A. Abragam, *The Principles of Nuclear Magnetism* (Clarendon Press, Oxford, England, 1961).

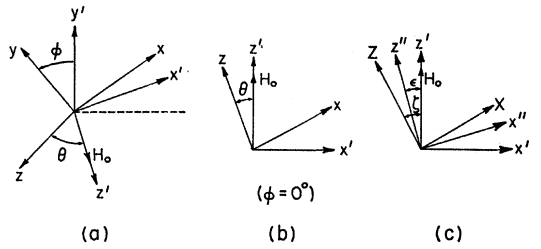

FIG. 7. (a) Orientation of xyz and $x'y'z'$ reference systems; (b) orientation of xyz and $x'y'z'$ reference systems: particular case for $\varphi=0°$; (c) orientation of XYZ, $x'y'z'$, and $x''y''z''$ reference systems used in the perturbation calculation.

then the nuclear spin is quantized in the direction of $\mathbf{H}_0$, and the eigenfunctions are eigenfunctions of $I_{z'}$ with eigenvalues m_I. Expressing I_x, I_y, I_z and S_x, S_y, S_z in terms of $I_{x'}$, $I_{y'}$, $I_{z'}$, and $S_{x'}$, $S_{y'}$, $S_{z'}$ and neglecting the off-diagonal terms, we obtain the eigenvalues for

$$E=\gamma_e\hbar H_0 m_S-\gamma_n\hbar H_0 m_I + m_S m_I(a+B_x h_x^2+B_y h_y^2+B_z h_z^2)$$
$$=\gamma_e\hbar H_0 m_S-\gamma_n\hbar H_0 m_I+W m_S m_I, \quad (13)$$

where h_x, h_y, and h_z are the direction cosines of $\mathbf{H}_0$ in the principal axes system. Electron transitions obey the selection rules $\Delta m_I=0$, $\Delta m_S=\pm 1$. Therefore, from Eq. (13) we obtain

$$\omega_e=\Delta E/\hbar=\gamma_e H_0+(W/\hbar)m_I. \quad (14)$$

Nuclear transitions, which are the ones observed in ENDOR, are subjected to the selection rules $\Delta m_S=0$, $\Delta m_I=\pm 1$. Thus,

$$\omega_n=\Delta E/\hbar=|\gamma_n H_0-(W/\hbar)m_S|. \quad (15)$$

To interpret this equation let us assume $S=\frac{1}{2}$. If $\gamma_n H_0>W/2\hbar$, two lines are expected at frequencies

$$\omega_n=\gamma_n H_0\pm W/2\hbar. \quad (16)$$

If $W/2\hbar>\gamma_n H_0$, two lines are observed at frequencies

$$\omega_n=W/2\hbar\pm\gamma_n H_0. \quad (17)$$

An examination of the spin Hamiltonian [Eq. (10)] show that this approximation is valid even when the assumption (12) does not hold, if $\mathbf{H}_0$ is parallel to one of the principal axes. If $\mathbf{H}_0$ is parallel to z, Eq. (16), for instance, becomes

$$\omega_n=\gamma_n H_0\pm A_z/2\hbar. \quad (18)$$

Therefore, it is possible to find the values of A_x, A_y, A_z by measuring the separation between the two lines when $\mathbf{H}_0$ is along the principal axes.

A. First-Order Correction to Nuclear Frequencies

It is important for the investigation reported in this paper to consider the case when assumption (12) does not hold. In this case there is a large field component perpendicular to $\mathbf{H}_0$ due to the dipolar interaction. The nuclear spin is then quantized along the resultant field and not along $\mathbf{H}_0$. We shall parallel Slichter's[3] derivation of the first-order correction that must be introduced in Eq. (13) for a slightly more general case. The orientation of the axes are shown in Fig. 7; x, y, and z are the principal axes of the hyperfine interaction and x', y', and z' is a system fixed with respect to $\mathbf{H}_0$ with z' parallel to $\mathbf{H}_0$. For the ENDOR nuclei considered in this paper it will be sufficient to consider the case of the plane of rotation of $\mathbf{H}_0$ containing at least one of the hyperfine principal axes. Therefore, in Fig. 7 y' is taken to be perpendicular to z. The angle φ is a rotation about the z axis of y away from y' and the θ is a rotation about y' of z' away from z. The Hamiltonian of Eq. (10) becomes

$$\mathcal{H}=\gamma_e\hbar H_0 S_{z'}-\gamma_n\hbar H_0 I_{z'}+A_x S_x I_x+A_y S_y I_y+A_z S_z I_z. \quad (19)$$

We continue to assume that the electron Zeeman term is larger than the hyperfine term, so that m_S is a good quantum number. Transforming electron and nuclear-spin components to the reference system of $\mathbf{H}_0$ and neglecting terms involving $S_{x'}$ and $S_{y'}$ which do not produce a first-order effect, we obtain in first order

$$\mathcal{H}=\gamma_e\hbar H_0 S_{z'}-\gamma_n\hbar H_0 I_{z'} + I_{z'}S_{z'}[(A_x\cos^2\varphi+A_y\sin^2\varphi)\sin^2\theta+A_z\cos^2\theta] + I_{y'}S_{z'}[(A_x-A_y)\sin\varphi\cos\varphi\sin\theta] + I_{x'}S_{z'}[(A_x\cos^2\varphi+A_y\sin^2\varphi-A_z)\sin\theta\cos\theta] \quad (20)$$

or

$$\mathcal{H}=\gamma_e\hbar H_0 S_{z'}-\gamma_n\hbar\mathbf{H}^e\cdot\mathbf{I}, \quad (21)$$

where the components of the effective field $\mathbf{H}^e$ are

$$H_{z'}{}^e=H_0-(1/\gamma_n\hbar)[(A_x\cos^2\varphi+A_y\sin^2\varphi)\times\sin^2\theta+A_z\cos^2\theta]S_{z'}$$
$$=H_0-(1/\gamma_n\hbar)W_1 S_{z'},$$
$$H_{x'}{}^e=-(1/\gamma_n\hbar)(A_x\cos^2\varphi+A_y\sin^2\varphi-A_z)\sin\theta\cos\theta S_{z'}$$
$$=-(1/\gamma_n\hbar)W_2 S_{z'},$$
$$H_{y'}{}^e=-(1/\gamma_n\hbar)(A_x-A_y)\sin\varphi\cos\varphi\sin\theta\, S_{z'}$$
$$=-(1/\gamma_n\hbar)W_3 S_{z'}. \quad (22)$$

The above equations define W_1, W_2, and W_3.

The nuclear transitions correspond to frequencies

$$\omega=\gamma_n H^e(m_S). \quad (23)$$

However,

$$H^e=\{[H_0-(1/\gamma_n\hbar)W_1 m_S]^2+[(1/\gamma_n\hbar)W_2 m_S]^2+[(1/\gamma_n\hbar)W_3 m_S]^2\}^{1/2}.$$

Therefore,

$$H^e \approx [H_0 - (1/\gamma_n\hbar) W_1 m_S] \times \left[1 + \frac{1}{2} \frac{(W_2 m_S)^2 + (W_3 m_S)^2}{(\gamma_n\hbar)^2 [H_0 - (1/\gamma_n\hbar) W_1 m_S]^2}\right]. \quad (24)$$

Combining (23) and (24), we obtain

$$\omega = \omega_0 + \Delta\omega, \quad (25)$$

where

$$\omega_0 = \gamma_n H_0 - (W_1/\hbar) m_S, \quad (26)$$

$$\Delta\omega = (m_S^2/2\omega_0)[(W_2^2/\hbar) + (W_3^2/\hbar)]. \quad (27)$$

When the magnetic field $\mathbf{H}_0$ is rotated in a principal plane of the hyperfine interaction, the first-order correction given by Eq. (27) becomes simpler. Let H_0 be on the zx plane [Fig. 7(b)]. Substituting $\varphi = 0$ in Eqs. (22) (this is the case given by Slichter[3]), we obtain

$$W_1 = A_x \sin^2\theta + A_z \cos^2\theta,$$

$$W_2 = (A_x - A_z) \sin\theta \cos\theta,$$

$$W_3 = 0, \quad (28)$$

and the first-order correction reduces to

$$\Delta\omega = (1/8\omega_0)(W_2/\hbar)^2, \quad \text{for} \quad S = \tfrac{1}{2}. \quad (29)$$

One observes that $\Delta\omega = 0$ for $\theta = 0°$ or $90°$, which justifies our previous remark that Eq. (16) may be used if H_0 is along one of the principal axes even when assumption (12) does not hold.

B. Dependence of ENDOR Frequencies on Nuclear Spin State of V_K Center

In this section we shall show how the ENDOR frequencies of the lattice nuclei depend on the nuclear spin state (denoted by M) of the two molecular nuclei of the V_K center. Equations (25), (26), and (29) are valid only for $M = 0$; for $M = \pm 1$ a correction must be introduced.

The effect may be explained by the fact that a nucleus near to the defect sees, instead of the applied dc field $\mathbf{H}_0$, an effective field $\mathbf{H}^e$ which depends on the nuclear spin state of the V_K center. The effect is somewhat similar to the one treated in Sec. III A, where it was shown that the axis of quantization of the nucleus was not along $\mathbf{H}_0$, but along an effective field dependent on the electron spin state (m_S). The discussion to be presented in this section incorporates these two effects, and it is as though the nuclear spin $\mathbf{I}$ of a lattice nucleus were quantized along an effective field $\mathbf{H}^e(m_S, M)$. Effects similar to those discussed here would also occur for sufficiently anisotropic g values when the magnetic field is not a good axis of quantization for the electron spin. However, the g anisotropy effects for the V_K center are ignored here because they are more than an order of magnitude smaller than the effects due to the anisotropy of the hyperfine interaction of the molecular nuclei.

The perturbation treatment of the effect will follow a simple scheme. The spin Hamiltonian is written as a sum of two terms:

$$\mathcal{H} = \mathcal{H}_{\text{ESR}} + \mathcal{H}_{\text{ENDOR}}. \quad (30)$$

$\mathcal{H}_{\text{ESR}}$ represents the interactions of the unpaired electron, the two fluorine nuclei of the molecule, and the applied dc magnetic field. $\mathcal{H}_{\text{ENDOR}}$ adds the interaction of a lattice nucleus with the electron and the applied dc magnetic field. The interaction of the electron with the two fluorines is much larger than the interaction with any of the lattice nuclei. Therefore we calculate the (spin) wave functions of the unpaired electron by a perturbation treatment, neglecting completely the effect of $\mathcal{H}_{\text{ENDOR}}$. In a second step we calculate the expectation values of $\mathcal{H}_{\text{ENDOR}}$ between the corrected wave functions leaving $\mathbf{I}$ (the spin of the lattice nucleus in question) as an operator. This allows us to define the effective magnetic field along which $\mathbf{I}$ is quantized. This treatment is equivalent to second-order perturbation theory. However, since the final equations are complicated and since Castner and Känzig[2] have already done the ESR part of the problem, it is more illuminating to use this two-step approach.

For the calculation of the wave function, we use the perturbation treatment of Castner and Känzig,[2] and the reader is referred to their paper for additional details. Their calculation is good when the angle ζ (Fig. 2) between the V_K center and the dc magnetic field varies from 0° to about 75°. For ζ larger than 75° the perturbation calculation breaks down and an exact diagonalization of the spin-Hamiltonian matrix as done by Woodruff and Känzig[7] is necessary.

Let X, Y, and Z be the principal axes of the hyperfine interaction of the electron with the two fluorines, and $\mathbf{H}_0$ be along the z' axis of the system $x'y'z'$ [Fig. 7(c)]. The ESR spectra are described by the axially symmetric spin Hamiltonian:

$$\mathcal{H}_{\text{ESR}} = g\beta_0 H_0 S_{z'} + a\mathbf{K}\cdot\mathbf{S} + bK_Z S_Z, \quad (31)$$

with

$$g = (g_{\parallel}^2 \cos^2\zeta + g_{\perp}^2 \sin^2\zeta)^{1/2}, \quad (32)$$

where $\mathbf{K}$ is the sum of the nuclear spin operators of the fluorine nuclei, $\mathbf{S}$ is the electron spin operator, g is the spectroscopic splitting factor of the V_K center, and β_0 is the Bohr magneton. The isotropic and anisotropic constants a and b and the g components $g_{\parallel}$ and $g_{\perp}$ are determined to fit the experimental data and were found to be[7]

$$|a|/g_0\beta_0 = 59 \text{ G}, \qquad g_{\parallel} = 2.0031,$$

$$(a+b)/g_0\beta_0 = 887 \text{ G}, \qquad g_{\perp} = 2.0230. \quad (33)$$

In the $x'y'z'$ system of reference the Hamiltonian

becomes

$$\mathcal{H}_{\mathrm{ESR}}=[g\beta_0H_0+(a+b\cos^2\zeta)K_{z'}-(b\sin\zeta\cos\zeta)K_{x'}]S_{z'}$$
$$+[(a+b\sin^2\zeta)K_{x'}-(b\sin\zeta\cos\zeta)K_{z'}]S_{x'}+aK_{y'}S_{y'}. \quad (34)$$

If we choose as basis functions the eigenfunctions of $K_{z'}$ and $S_{z'}$, we observe that there are terms diagonal in m_S which are off-diagonal in M ($m_S=\langle S_{z'}\rangle$ and $M=\langle K_{z'}\rangle$). A new system $x''y''z''$ is introduced for the nuclear operators, and the angle ϵ [Fig. 7(c)] between z'' and z' is chosen to make the term diagonal in m_S also diagonal in M. Equation (34) becomes

$$\mathcal{H}_{\mathrm{ESR}}=g\beta_0H_0S_{z'}-[(a\sin\epsilon+b\sin^2\zeta$$
$$\times\sin\epsilon+b\sin\zeta\cos\zeta\cos\epsilon)K_{z''}$$
$$-(a\cos\epsilon+b\sin^2\zeta\cos\epsilon-b\sin\zeta\cos\zeta\sin\epsilon)K_{x''}]S_{x'}$$
$$+aK_{y''}S_{y'}+[(a\cos\epsilon+b\cos^2\zeta\cos\epsilon+b\sin\zeta\cos\zeta\sin\epsilon)K_{z''}$$
$$+(a\sin\epsilon+b\cos^2\zeta\sin\epsilon-b\sin\zeta\cos\zeta\cos\epsilon)K_{x''}]S_{z'}. \quad (35)$$

Now, if we choose

$$\tan\epsilon=(b\sin\zeta\cos\zeta)/(a+b\cos^2\zeta),$$

the off-diagonal term $K_{x''}S_{z'}$ is eliminated and the spin Hamiltonian becomes

$$\mathcal{H}_{\mathrm{ESR}}=[g\beta_0H_0+(p^2+q^2)^{1/2}K_{z''}]S_{z'}-\frac{(2a+b)q}{(p^2+q^2)^{1/2}}K_{z''}S_{x'}$$
$$+\frac{a(a+b)}{(p^2+q^2)^{1/2}}K_{x''}S_{x'}+aK_{y''}S_{y'}$$
$$=\mathcal{H}_0+V_1+V_2+V_3, \quad (36)$$

with

$$p=a+b\cos^2\zeta, \qquad q=b\sin\zeta\cos\zeta, \qquad \tan\epsilon=q/p. \quad (37)$$

The first term, $\mathcal{H}_0$, is diagonal in m_S and M. The second term, V_1, is diagonal in M and off diagonal in m_S; it constitutes the largest perturbation. The third term, V_2, is off diagonal in m_S and M, and it is very small[2] except for ζ near $\frac{1}{2}\pi$. The fourth term, V_3, is very small in comparison with V_1 and V_2, and it is neglected.

We start with eigenfunctions $|m_S, M\rangle$ of $\mathcal{H}_0$ and want to calculate the eigenfunctions $\psi_{m_S,M}$ of $\mathcal{H}_{\mathrm{ESR}}$ by first-order perturbation theory:

$$\psi_n^{(1)}=\sum_m[V_{mn}/(E_n^0-E_m^0)]\psi_m^{(0)}. \quad (38)$$

Thus,

$$\psi_{1/2,M}^{(1)}=\frac{\langle-\frac{1}{2}M\,|\,V_1\,|\,+\frac{1}{2}M\rangle}{E_{1/2,M}-E_{-1/2,M}}\,|\,-\tfrac{1}{2},M\rangle$$
$$+\frac{\langle-\frac{1}{2}M-1\,|\,V_2\,|\,\frac{1}{2}M\rangle}{E_{1/2,M}-E_{-1/2,M-1}}\,|\,-\tfrac{1}{2},M-1\rangle$$
$$+\frac{\langle-\frac{1}{2}M+1\,|\,V_2\,|\,\frac{1}{2}M\rangle}{E_{1/2,M}-E_{-1/2,M+1}}\,|\,-\tfrac{1}{2},M+1\rangle. \quad (39)$$

An analogous expression may be written for $\psi_{-1/2,M}^{(1)}$. Therefore,

$$\psi_{1/2,M}=|\,\tfrac{1}{2},M\rangle-\alpha\,|\,-\tfrac{1}{2},M\rangle+\lambda_1\,|\,-\tfrac{1}{2},M-1\rangle$$
$$+\lambda_2\,|\,-\tfrac{1}{2},M+1\rangle, \quad (40a)$$

$$\psi_{-1/2,M}=|\,-\tfrac{1}{2},M\rangle+\alpha\,|\,+\tfrac{1}{2},M\rangle-\lambda_1\,|\,+\tfrac{1}{2},M-1\rangle$$
$$-\lambda_2\,|\,+\tfrac{1}{2},M+1\rangle, \quad (40b)$$

where

$$\alpha=\frac{(2a+b)q}{2(p^2+q^2)^{1/2}}\frac{M}{[g\beta_0H_0+(p^2+q^2)^{1/2}M]}, \quad (41)$$

$\lambda_1=0$ for $M=-1$ and $\lambda_2=0$ for $M=+1$.

Otherwise,

$$\lambda_1=\tfrac{1}{4}\sqrt{2}[a(a+b)/(p^2+q^2)^{1/2}]$$
$$\times[g\beta_0H_0+\tfrac{1}{2}(2M-1)(p^2+q^2)^{1/2}]^{-1}, \quad (42a)$$

$$\lambda_2=\tfrac{1}{4}\sqrt{2}[a(a+b)/(p^2+q^2)^{1/2}]$$
$$\times[g\beta_0H_0+\tfrac{1}{2}(2M+1)(p^2+q^2)^{1/2}]^{-1}. \quad (42b)$$

Let x, y, and z be the principal axes of the hyperfine interaction of a lattice nucleus and the unpaired electron spin. We assume that one of the axes of the x, y, z system is parallel to one of the axes of the V_K center. This is the case for all the nuclei we have studied from A to F. We take the magnetic field to be on the xz plane (i.e., take a specific case of $y\,||\,Y\,||\,y'$) [Fig. 7(b)]. The more general case of $\varphi\neq0$ has been derived but the additional complexity of the equations tends to obscure the main points of the dependence of the ENDOR on the spin state M. The ENDOR Hamiltonian is

$$\mathcal{H}_{\mathrm{ENDOR}}=-\psi_n\hbar H_0I_{z'}+A_xI_xS_x+A_yI_yS_y+A_zI_zS_z, \quad (43)$$

where I is the nuclear spin of a lattice nucleus near the V_K center and γ_n is the gyromagnetic ratio for the nucleus. Transforming electron and nuclear spin coordinates to the $x'y'z'$ reference system, we obtain

$$\mathcal{H}_{\mathrm{ENDOR}}=[-\gamma_n\hbar H_0+(A_x\sin^2\theta+A_z\cos^2\theta)S_{z'}$$
$$+(A_x-A_z)\sin\theta\cos\theta S_{x'}]I_{z'}+[(A_x-A_z)\sin\theta\cos\theta S_{z'}$$
$$+(A_x\cos^2\theta+A_z\sin^2\theta)S_{x'}]I_{x'}+A_yS_{y'}I_{y'}$$
$$=[-\gamma_n\hbar H_0+W_1S_{z'}+W_2S_{x'}]I_{z'}$$
$$+[W_2S_{z'}+W_1'S_{x'}]I_{x'}+A_yS_{y'}I_{y'}, \quad (44)$$

with

$$W_1=A_x\sin^2\theta+A_z\cos^2\theta,$$
$$W_2=(A_x-A_z)\sin\theta\cos\theta,$$
$$W_1'=A_x\cos^2\theta+A_z\sin^2\theta. \quad (45)$$

We now calculate the expectation values of $\mathcal{H}_{\mathrm{ENDOR}}$ in the states $\psi_{m_S,M}$ given by Eqs. (40a) and (40b), leaving the nuclear spin **I** as an operator. If we neglect

all terms containing α^2, λ_1^2, and λ_2^2, we obtain

$$\begin{aligned}\mathcal{H}_{\text{ENDOR}}(I) &= \langle \psi_{\pm 1/2,M} \mid \mathcal{H}_{\text{ENDOR}} \mid \psi_{\pm 1/2,M} \rangle \\ &= \langle \pm\tfrac{1}{2}, M \mid \mathcal{H}_{\text{ENDOR}} \mid \pm\tfrac{1}{2}, M \rangle \\ &\quad \mp\alpha \langle \pm\tfrac{1}{2}, M \mid \mathcal{H}_{\text{ENDOR}} \mid \mp\tfrac{1}{2}, M \rangle \\ &\quad \mp\alpha \langle \mp\tfrac{1}{2}, M \mid \mathcal{H}_{\text{ENDOR}} \mid \pm\tfrac{1}{2}, M \rangle. \end{aligned} \quad (46)$$

Substituting (44) into (46) and calculating the matrix elements, we obtain

$$\begin{aligned}\mathcal{H}_{\text{ENDOR}}(I) &= [-\gamma_n\hbar H_0 + W_1 m_S - 2m_S\alpha W_2] I_{z'} \\ &\quad + [W_2 m_S - 2m_S\alpha W_1'] I_{x'} \\ &= -\gamma_n\hbar \mathbf{H}^e \cdot \mathbf{I}. \end{aligned} \quad (47)$$

It is as though the nucleus were coupled to an effective field $\mathbf{H}^e$ with components

$$\begin{aligned} H_{z'^e}(m_S, M) &= H_0 - (W_1 m_S/\gamma_n\hbar) + (2m_S\alpha W_2/\gamma_n\hbar), \\ H_{x'^e}(m_S, M) &= -(W_2 m_S/\gamma_n\hbar) + (2m_S\alpha W_1'/\gamma_n\hbar), \\ H_{y'^e}(m_S, M) &= 0. \end{aligned} \quad (48)$$

Thus,

$$\begin{aligned} H_{\text{eff}} &= \left[\left(H_0 - \frac{W_1 m_S}{\gamma_n\hbar} + \frac{2m_S\alpha W_2}{\gamma_n\hbar}\right)^2 \right. \\ &\quad \left. + \left(-\frac{W_2 m_S}{\gamma_n\hbar} + \frac{2m_S\alpha W_1'}{\gamma_n\hbar}\right)^2\right]^{1/2} \\ &\approx \left(H_0 - \frac{W_1 m_S}{\gamma_n\hbar} + \frac{2m_S\alpha W_2}{\gamma_n\hbar}\right) \\ &\quad \times \left[1 + \frac{1}{2}\left(\frac{-W_2 m_S + 2m_S\alpha W_1'}{\gamma_n\hbar H_0 - W_1 m_S + 2m_S\alpha W_2}\right)^2\right]. \end{aligned} \quad (49)$$

The nuclear transitions are given by

$$\hbar\omega = \gamma_n\hbar H_{\text{eff}}(m_S, M). \quad (50)$$

Substituting (49) in (50), we obtain

$$\omega^{(1)} = \omega^{(0)} + \Delta\omega, \quad (51)$$

where

$$\omega^{(0)} = \gamma_n H - (W_1 m_S/\hbar) + (2\alpha W_2 m_S/\hbar), \quad (52)$$

$$\omega^{(0)}\Delta\omega = \tfrac{1}{2}[-(W_2 m_S/\hbar) + (2\alpha W_1' m_S/\hbar)]^2. \quad (53)$$

For ζ near 90°, off-diagonal terms of the spin matrix which were not introduced in the perturbation calculation become large and this treatment breaks down. In this case a numerical calculation of the wave functions of the spin Hamiltonian $\mathcal{H}_{\text{ESR}}$ was carried out. The perturbed wave functions of Eqs. (40a) and (40b) were replaced by the new numerical wave functions and the remaining steps of the calculation were repeated.

The numerical calculation of the wave functions followed closely the work of Woodruff and Känzig.[7] We add to the Hamiltonian of Eq. (34) a nuclear Zeeman term $\gamma_F\hbar H_0 K_{z'}$. As basis functions we take the set $\mid S, m_S\rangle \mid K, M\rangle$, where $\mid K, M\rangle$ stands for triplet and singlet combinations of the nuclear spin functions of the fluorine nuclei in the molecular ion:

$$\begin{aligned} \mid 1'\rangle &= \mid \tfrac{1}{2}, \tfrac{1}{2}\rangle \mid 1, 1\rangle, & \mid 5'\rangle &= \mid \tfrac{1}{2}, -\tfrac{1}{2}\rangle \mid 1, 0\rangle, \\ \mid 2'\rangle &= \mid \tfrac{1}{2}, \tfrac{1}{2}\rangle \mid 1, 0\rangle, & \mid 6'\rangle &= \mid \tfrac{1}{2}, -\tfrac{1}{2}\rangle \mid 1, 1\rangle, \\ \mid 3'\rangle &= \mid \tfrac{1}{2}, \tfrac{1}{2}\rangle \mid 1, -1\rangle, & \mid 7'\rangle &= \mid \tfrac{1}{2}, \tfrac{1}{2}\rangle \mid 0, 0\rangle, \\ \mid 4'\rangle &= \mid \tfrac{1}{2}, -\tfrac{1}{2}\rangle \mid 1, -1\rangle, & \mid 8'\rangle &= \mid \tfrac{1}{2}, -\tfrac{1}{2}\rangle \mid 0, 0\rangle. \end{aligned} \quad (54)$$

The matrix $[\langle i' \mid \mathcal{H}_{\text{ESR}} \mid j'\rangle]$ is an 8×8 matrix. The matrix consists of one 6×6 block and one 2×2 block which is already diagonal. The states $\mid 7'\rangle$ and $\mid 8'\rangle$ are not mixed with other states. The transition between them gives the line R_3 of the ESR spectrum, which as we can see in Fig. 2 is independent of ζ. Any ENDOR observed in this line should be completely free of the effect discussed in this section.

A program was prepared to diagonalize the 6×6 block and to calculate the transformation matrix. The eigenstates of $\mathcal{H}_{\text{ESR}}$ are immediately constructed in the form

$$\mid i\rangle = \sum_{j'=1}^{6} c_{j'} \mid j'\rangle, \quad (55)$$

with i varying from 1 to 6.

The ESR transitions occur between pairs of eigenstates $\mid i\rangle$. We now select the eigenstates corresponding to the ESR line which we are observing, and using Eq. (43) we calculate

$$\begin{aligned}\mathcal{H}_{\text{ENDOR}}(I) &= \langle i \mid \mathcal{H}_{\text{ENDOR}} \mid i\rangle \\ &= d_x I_x + d_y I_y + d_z I_z. \end{aligned} \quad (56)$$

At first because of the six terms of $\mathcal{H}_{\text{ENDOR}}$ and the six components of $\mid i\rangle$ one should expect 216 terms in (56). However, most of the terms vanish because of orthogonality of the basis states. From Eq. (56) $\mathbf{H}^e$ is defined, and finally, the frequency ω of the nuclear transition is calculated:

$$\omega = (d_x^2 + d_y^2 + d_z^2)^{1/2}/\hbar. \quad (57)$$

IV. RESULTS AND DISCUSSION

The theory developed in Sec. III predicts a dependence of the ENDOR frequencies on the nuclear spin state of the V_K center. In fact, this effect was observed. While the frequencies of the ENDOR lines observed on the $R_3(M=0)$ ESR line agree very well with Eqs. (25)–(27), the results obtained on lines R_1 and $R_4(M=\pm 1)$ differ by as much as 20 times the experimental error, and are in good agreement with Eqs. (51)–(53). We shall leave the discussion of this effect for Sec. IV C.

For nuclei B, C, D, and E the direction of one of the principal axes of the hyperfine interaction tensor is known from symmetry considerations, but the direc-

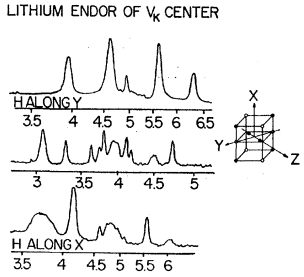

FIG. 8. Lithium ENDOR spectra for H_0 parallel to the principal axes of the V_K center.

tions of the two other axes are unknown *a priori*, and are determined from the ENDOR measurements. Whenever possible the directions of the principal axes and the values of the hyperfine interaction constants (A_x, A_y, and A_z of Sec. III) should be determined from measurements made on the R_3 line, where the effect of the nuclear spin state of the V_K center vanishes. This brings about the first difficulty, because V_K centers of different orientations have overlapping R_3 lines. Therefore, the ENDOR spectrum obtained on the R_3 line will be a superposition of spectra.

Another difficulty encountered was in the number of centers that could be produced. It was observed that the ENDOR signal is very strong for $\zeta=0°$ or $\zeta=90°$ (ζ is the angle between $\mathbf{H}_0$ and the axis of the V_K center) but is weaker for intermediate values of ζ. Therefore, to obtain a complete angular dependence of the ENDOR spectrum, which is necessary for an unambiguous identification of the lines, a large amount of centers must be produced. The number of V_K centers one may form is limited by the electron traps available. Very efficient electron traps are known for other alkali halides[2,4] but none of them proved very helpful for LiF. The best doping that we found was AgF_2. Another paramagnetic center as well as the V_K center was formed (Fig. 1), but it had no ENDOR at 90°K and did not interfere with our measurements.

The two difficulties were solved successfully by reorienting the V_K centers as discussed in Sec. II. The number of V_K centers of one orientation was enhanced by approximately a factor of 3 (Fig. 1). The numbers of centers of other orientation are greatly reduced and do not give observable ENDOR signals for the R_3 line.

The results show that the hole is very well localized and the hyperfine interaction with neighboring nuclei is

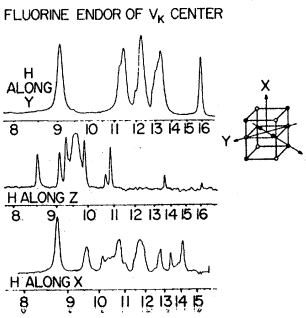

FIG. 9. Fluorine ENDOR spectra for H_0 parallel to the principal axes of the V_K center.

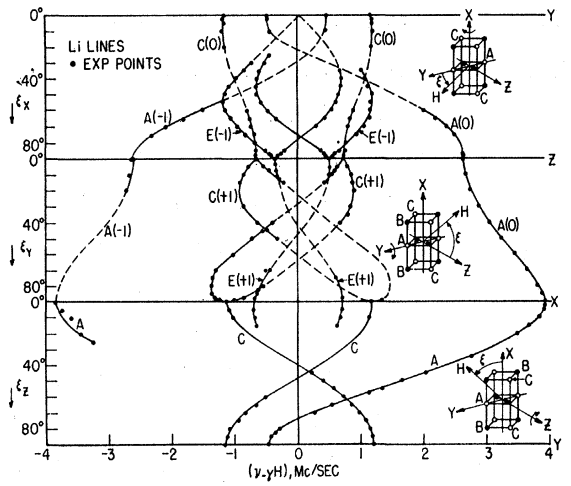

FIG. 10. Angular dependence of hyperfine interaction of surrounding lithium nuclei. The arrow on one of the principal axes indicates the axis of rotation of the sample.

quite small. The conditions $W_{\text{hfs}}/(2\hbar)<\gamma_F H_0$ and $W_{\text{hfs}}/(2\hbar)<\gamma_{Li}H_0$, where γ_F and γ_{Li} are the gyromagnetic ratios for fluorine and lithium, are fulfilled. Therefore, Eq. (16) holds. It is expected that for each fluorine nucleus there is a pair of lines symmetric with respect to $\gamma_F H_0$. This immediately separates the spectrum into a lithium spectrum and a fluorine spectrum. There is some overlapping of lines for certain orientations of the magnetic field, but it is very easy to distinguish to what species they belong by searching for the high-frequency mate in the F spectrum.

The large anisotropy of the V_K center and the small interaction of the unpaired electron with neighboring nuclei make the identification of lines difficult. Many lines are in a low-frequency range, and there are many

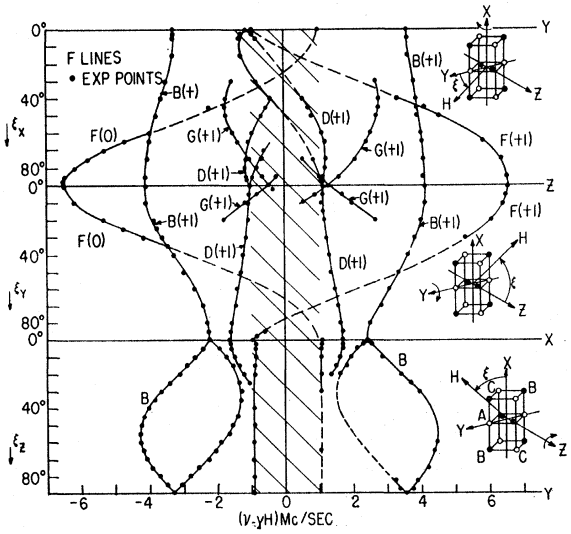

FIG. 11. Angular dependence of hyperfine interaction of surrounding fluorine nuclei.

crossings when the crystal is rotated in the dc magnetic field. Besides, the dynamics of ENDOR are complicated, and the intensities of the lines do not always show a simple relation to the number of equivalent nuclei responsible for them. To obtain an unambiguous identification of lines it was necessary to make three sets of measurements. Let X, Y, and Z be the principal axes of the V_K center; Z is the molecular axis, and X is the principal axis that coincides with the [100] crystal axis. It must be recalled that in our apparatus the sample is rotated and $\mathbf{H}_0$ is kept constant in a direction perpendicular to the axis of rotation. However, we shall speak of rotation of $\mathbf{H}_0$, and the angle that determines the position of $\mathbf{H}_0$ will be such that $\mathbf{H}_0$ is rotating clockwise in the reference system XYZ (Figs. 10 and 11). The three sets of measurements are the following:

(1) Rotation of $\mathbf{H}_0$ in plane YZ; V_K centers oriented in a [110] direction; sample rotated around [001].

(2) Rotation of $\mathbf{H}_0$ in plane XZ; V_K centers oriented in a [110] direction; sample rotated around [110].

(3) Rotation of $\mathbf{H}_0$ in plane XY; V_K centers oriented in a [110] direction; sample rotated around [110].

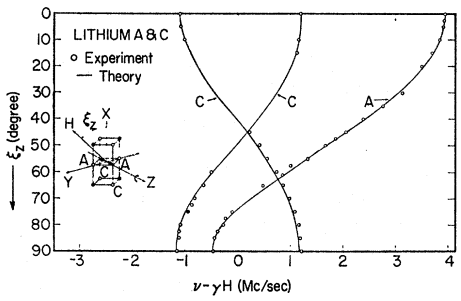

FIG. 12. Calculated [Eqs. (25), (26), and (29)] and experimental angular variations of hyperfine interaction for lithium A and C for the R_3 ESR line.

Figures 8 and 9 show the Li and F spectra for the magnetic field along the three principal axes of the V_K center. All of this work refers to Li^7 (92.6% natural abundance); ENDOR lines due to Li^6 (7.4% natural abundance) were not observed.

A. Identification of Lines

To identify the lines the frequencies were plotted against the angles ξ_i ($i=X$, Y, Z) that determine the position of $\mathbf{H}_0$ with respect to the principal axes of the V_K center. The subindex ξ_i indicates the axis of rotation. For instance, for $\mathbf{H}_0$ rotating in the plane YZ, ξ_X is the angle between Y and $\mathbf{H}_0$. Except when Z is the axis of rotation and ζ is always 90°, ζ varies with ξ. Therefore, for different values of ξ the ESR signal occurs for different magnetic fields and $\gamma_n H_0$ of Eq. (16) has an angular dependence. However, we are interested only in the angular dependence of the hyperfine interaction. Thus, instead of plotting measured frequencies we plot

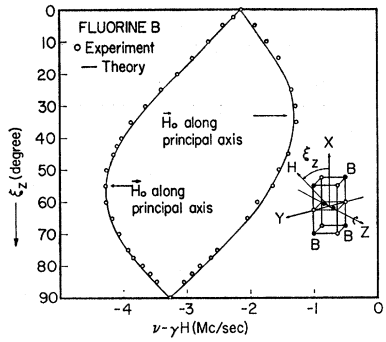

FIG. 13. Calculated [Eqs. (25), (26), (29)] and experimental angular variations of hyperfine interaction for fluorines B for rotation around Z for the R_3 ESR line.

$\nu-\gamma_n H_0$. Also, ξ is not in general equal to θ because the principal axes of the hyperfine interaction of the lattice nuclei are not in general parallel to the principal axes of the V_K center.

Figures 10 and 11 show the angular variation of Li and F spectra. ENDOR measurements obtained on different ESR lines were used and this is indicated by the value of M in parentheses. The nuclei surrounding the V_K center are identified by letters A to G in accordance with their distance to the center of the defect. This is shown in Fig. 4.

When we refer to symmetry of the lattice in the following discussion we mean the local symmetry in the neighborhood of the imperfection. It is obvious that this local symmetry is lower than the symmetry of the perfect lattice because of the lower symmetry of the V_K center. The origin is the center of the imperfection. It may be seen that the Hamiltonian of Eq. (10) is invariant with respect to an inversion in the origin and that the center of the V_K center is a center of inversion of the lattice. Therefore, the nuclei which are transformed into each other by an inversion in the origin are physically equivalent for all directions of $\mathbf{H}_0$. Also, the Hamiltonian of Eq. (10) is invariant with respect to a reflection in a plane of local symmetry if this plain contains $\mathbf{H}_0$. If a nucleus is mapped into another of the

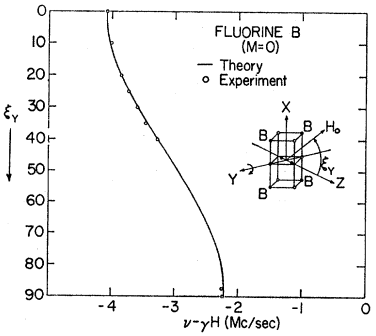

FIG. 14. Calculated [Eqs. (25)–(27)] and experimental angular variations of hyperfine interaction for fluorines B for rotation around Y for the R_3 ESR line.

TABLE I. Principal-axes (x, y, z) hyperfine values[a] in Mc/sec and orientations (α, β, γ) with respect to the V_K principal axes (X, Y, Z).

Nucleus	A_x	A_y	A_z	α	β	γ
A(Li)	−8.060±0.005	+1.020±0.005	−5.320±0.008	0°	0°	0°
B(F)	−2.840±0.012	−9.055±0.012	−8.170±0.008	34° ±1°	34° ±1°	0°
C(Li)	+2.800±0.010	−2.450±0.006	−1.820±0.010	17° ±1°	0°	17° ±1°
D(F)	−3.390±0.014	+2.710±0.012	−2.360±0.012	0°	12° ±1°	12° ±1°
E(Li)	−1.470±0.010	−1.370±0.008	+2.360±0.008	0°	39° ±1°	39° ±1°
F(F)	−2.090±0.006	−2.050±0.006	+13.020±0.006	0°	0°	0°

[a] See Ref. 21.

same kind by such an operation, the two nuclei are equivalent. Therefore, for rotations of $\mathbf{H}_0$ in principal planes of the V_K center, certain groups of ions become physically equivalent and their ENDOR lines superpose. An inspection of Figs. 10 and 11 based on the preceding discussion allows the establishment of a firm correspondence between the ENDOR lines and the nuclei labeled A to G as shown in Fig. 4.

The two lithium nuclei labeled A are equivalent for any direction of $\mathbf{H}_0$. There is only one line (and the mate) in the lithium spectrum that does not split and this has been labeled A.

The fluorine nuclei labeled F also are equivalent for any direction of $\mathbf{H}_0$. For a rotation around Z that contains the F nuclei there should be only a very small angular variation because of the approximate axial symmetry of the V_K center around Z. This behavior is shown by the line labeled F.

The four lithium nuclei labeled C are equivalent for rotations around Z and X but split into two pairs of equivalent nuclei for rotation around Y.

The four fluorine nuclei labeled B are equivalent for rotations around X and Y but split into two pairs of equivalent nuclei for rotations around Z.

The four fluorine (lithium) nuclei labeled D (E) are equivalent for rotations around Z and Y, but split into two pairs for rotations around X.

Finally, the eight fluorine nuclei labeled G are equivalent only for $\mathbf{H}_0$ along the X, Y, and Z directions. For rotations around X, Y, and Z, they split into two sets of four equivalent nuclei. We observe that lines labeled G show this behavior for rotations around X and Y. The results were not good enough to establish a correspondence between lines of the third set of measurements and the nuclei G [see Ref. 20 for more details of the G nuclei in NaF].

[20] (a) D. Daly and R. Mieher, following paper, Phys. Rev. **175**, 412 (1968); (b) D. Daly and R. Mieher, Phys. Rev. Letters **19**, 637 (1967); (c) D. Daly and R. Mieher, Phys, Rev. (to be published).

The above analysis was based on the assumption that the accepted model for the V_K center was correct. However, the possibility of establishing such a correspondence between the lines and the surrounding nuclei of the defect proves the validity of the model. All trials made to fit a different model to these results have failed.

B. Determination of Principal Axes of Hyperfine Interaction and Hyperfine Interaction Constants. Comparison of Experiment and Theory

The principal axes of the hyperfine interaction of neighboring nuclei with the unpaired electron are not all determined by symmetry, except for the nuclei A and F. The following observation is helpful in their determination. If there is a plane of "local symmetry" containing the nucleus in question, one of the principal axes is perpendicular to this plane and the other two are therefore in this plane. Consequently, if $\mathbf{H}_0$ is rotated in this plane the hyperfine interaction should go through a maximum or a minimum when $\mathbf{H}_0$ is along each of the principal axes.

Let x, y, and z be the principal axes of the hyperfine interaction, and α, β, and γ the angles of x, y, z with X, Y, Z, respectively. For the lithium labeled A it may be concluded from the local symmetry of the lattice, that x, y, and z are parallel to X, Y, and Z. The hyperfine interaction constants A_x, A_y, and A_z, according to Eq. (18), may be obtained by measuring the separation of the mate lines for $\mathbf{H}_0$ along X, Y, and Z. The angular dependence of the ENDOR line when $\mathbf{H}_0$ is rotated in the XY plane is predicted by Eqs. (25), (26), and (29), and a comparison between theory and experimental values is shown in Fig. 12.

For the fluorines marked B the z axis is parallel to Z, because XY is a plane of symmetry. The direction of the second principal axis is now found in two steps. An inspection of the angular dependence of the lines (Fig. 13) for $\mathbf{H}_0$ rotating in the XY plane shows a maximum of the hyperfine interaction for $\alpha \approx 35°$, and

A_x, A_y, A_z are measured for $\mathbf{H}_0$ along x, y, z. A theoretical plot of the angular dependence is made, and by comparison with the experimental results the value of α is corrected to $\alpha=34°$. A comparison of theory and experiment for rotation around Z is shown in Fig. 13. For rotation around Y $\mathbf{H}_0$ is not in a principal plane of the hyperfine tensor but the rotation plane does contain one principal axis and the Eqs. (25) to (27) may be used; a comparison of theory and experiment is shown in Fig. 14.

The determination of the principal axes and the hyperfine interaction constants for nuclei C to F follows a similar pattern and the results are shown in Table I.[21,22] Comparison of theory and experiment is shown in Fig. 12 for lithium C and in Fig. 17 for fluorines F.

C. Dependence of ENDOR Frequencies on Nuclear Spin State of V_K Center

As we have pointed out before, frequency shifts were found between ENDOR lines observed for different

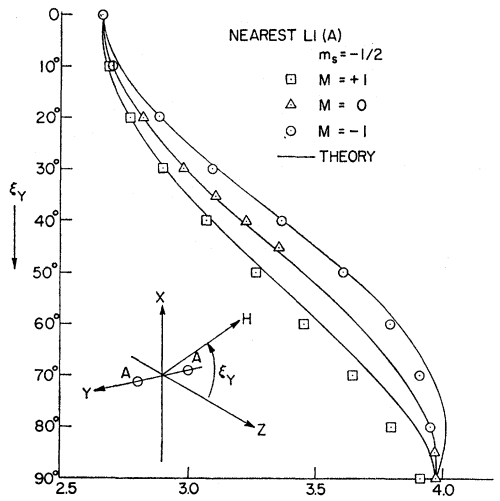

FIG. 15. Calculated [Eqs. (51)–(53)] and experimental angular variation of the hyperfine interaction of lithium A for $M=\pm1, 0$.

ESR lines. Measurements made on the R_3 line ($M=0$) are in very good agreement with Eqs. (25)–(27), which neglect the effect of the nuclear spin state of the V_K center. However, measurements made on the $R_1(M=+1)$ and $R_4(M=-1)$ lines show shifts in frequency as large as 3%, the experimental error being of the order of 0.2%. These shifts are well explained by the calculations developed in Sec. III B.

[21] Some of the values in Table I are slightly different from those listed in Ref. 6. These new values are based on new measurements by Y. H. Chu, Purdue University, and on a more detailed computer solution of the spin Hamiltonian as discussed in Refs. 20(a) and 22.

[22] I. Bass and R. Mieher, second following paper, Phys. Rev. **175**, 421 (1968).

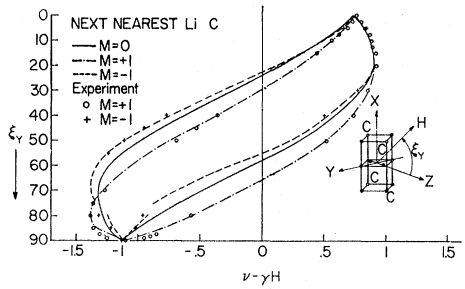

FIG. 16. Calculated and experimental angular variation of the hyperfine interaction of lithium C for $M=\pm1, 0$. Equations (51)–(53) have been used; however, when $M=-1$ for $\xi>80°$, the numerical computation of the wave function was used.

The effect is clear for lithium nuclei A and C and fluorine nuclei F. Comparisons between the angular variation, calculated by Eqs. (51)–(53), and the experimental points are shown in Figs. 15–17. The perturbation calculation is not accurate for $\xi\gtrsim75°$. A numerical calculation of the eigenfunctions and eigenvalues of the spin-Hamiltonian matrix was carried out on an IBM 7090 computer. The angular variation was then calculated by Eqs. (55)–(57) for the C nuclei for which the perturbation results were especially bad. The dashed curve shown in Fig. 16 for $M=-1$ and $\xi>80°$ is the result of this calculation.

D. Contact Part of Hyperfine Interaction and Exchange Polarization

The nuclear principal-axes hyperfine constants for six groups of nuclei are given in Table I along with the orientations of the nuclear principal axes with respect to the principal axes of the V_K center. The signs of the hyperfine constants were determined by assuming that the angular dependence is due to the dipole-dipole interaction between the nuclei and the unpaired electron. The isotropic contact part of the hyperfine interaction is $a_c=\frac{1}{3}(A_x+A_y+A_z)$. The experimental a_c values are listed in column 2 of Table II.

It was discussed in the Introduction that the unpaired spin of the F_2^- molecule is in a σ_u molecular orbit. A single contour of the electron density of the σ_u orbit is

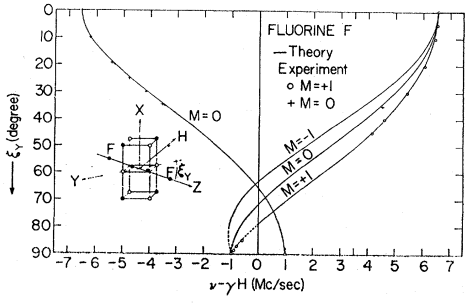

FIG. 17. Calculated [Eqs. (51)–(53)] and experimental angular variation of the hyperfine interaction of fluorines F for $M=\pm1, 0$.

TABLE II. Comparison of calculated contact part of hyperfine interactions with experimental values.

Nucleus	a_c (expt)	a_c (unpol)	a_c (pol)
A(Li)	−4.12	0	−15.35
B(F)	−6.69	0	−19.22
C(Li)	−0.49	+1.35	−2.71
D(F)	−1.01	+1.29	−5.31
E(Li)	−0.16	+6.36	+4.08
F(F)	+2.96	+7.17	+4.79

represented in Fig. 18 as two $2p$ atomic orbits. Because the center of the molecule is a point of inversion symmetry for the entire lattice, the XY plane (containing nuclear groups A and B) will be a nodal plane for the "true" σ_u orbit. A plane containing the C and D nuclei will not be an exact nodal plane because of the relaxation of the F_2^- molecule and because of S atomic orbital admixture into σ_u.

However, it will be noticed in Table II that the A and B nuclei in the σ_u nodal plane have large, negative contact interactions, i.e., the spin density $|\psi(r_n)|^2$, on a given nucleus points in a direction opposite to that of the unpaired σ_u electron. There are at least four mechanisms that could produce a nonzero contact interaction for the A and B nuclei.

(1) If the center of the molecule were not a point of inversion symmetry, then the XY plane would no longer be a rigorous nodal plane of σ_u. The only mechanism that could destroy the inversion symmetry and still be consistent with the rest of the ENDOR data would be lattice vibrations. There should then be a temperature dependence of this interaction. Measurements at 40 and 90°K show no temperature dependence greater than the experimental accuracy of ±0.2%.

(2) The g shift of the V_K center has been explained[2] as due to the spin-orbit coupling mixing some π_u with the σ_u (Fig. 3). Since the XY plane is not a nodal plane of the π_u orbit, this could result in a nonzero spin density at the A and B nuclei. However, the amount of the π_u admixture is known from the experimental g shift. The resulting spin density is 2 orders of magnitude too small.

Negative contact interactions due to exchange polarization of closed S shells are known to occur for the nuclei of magnetic ions and atoms in gases and solids.[23,24] Similar effects are also observed in free radicals.[25] There are two ways for exchange polarization to contribute to the contact interaction of the lattice nuclei.

(3) There will be an overlap of the σ_u orbit with the surrounding ions even if the spin density goes to zero at the nuclei. The ions will be polarized by the exchange interaction with the overlapping spin density. An order-of-magnitude estimate of this effect can be made by assuming that the polarization is proportional to the amount of overlap. It is known that divalent transition ions have a negative contact interaction roughly proportional to the number of unpaired d electrons.[23] Also, Shulman[26] has observed a negative contact interaction for F nuclei in K_2NaCrF_6. The amount of $2p$ character of the unpaired spin on the F^- ion as determined from the anisotropic part of the fluorine nuclear resonance was 4.9%. The exchange polarization contact interaction for the fluorine atom is 149 Mc/sec.[24,27] Therefore, a crude guess of the exchange polarization of the F^- ions in K_2NaCrF_6 would be 7.3 Mc/sec; Shulman observed 9.9 Mc/sec. However, this mechanism cannot explain the observed a_c values for the V_K center. For instance, the A lithium nuclei have $a_c = -4.12$ Mc/sec, whereas the experimental contact interaction for the lithium atom in the $(1s)^2 2p$ state is 10.5±0.3 Mc/sec.[28,29] The other contact values are also too large to explain by overlap polarization.

(4) The following mechanism gives the correct order-of-magnitude explanation of the a_c values in Table II. At least one of the closed shell $2p$-type orbitals (σ_g, π_u, and π_g) will have nonzero values of $|\psi(r_n)|^2$ at all of the surrounding lattice nuclei. If these orbitals are polarized by an exchange interaction with the unpaired σ_u electron there will be a nonzero (in most cases negative) spin density at all nuclei.

A crude estimate of this effect has been made using the following approximations.[30] The σ_u molecular orbit

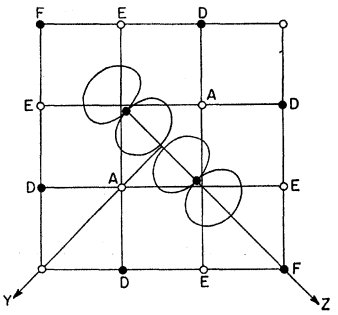

FIG. 18. The unpaired spin is in a σ_u molecular orbit represented here as two $2p_z$ atomic orbit contours.

[23] R. E. Watson and A. J. Freeman, Phys. Rev. **120**, 1125 (1960); **120**, 1134 (1960); **123**, 2027 (1961); **127**, 2058 (1962).
[24] D. A. Goodings, Phys. Rev. **123**, 1706 (1961).
[25] M. Karplus and G. K. Fraenkel, J. Chem. Phys. **35**, 1312 (1961), and references therein.
[26] R. G. Shulman and K. Knox, Phys. Rev. Letters **4**, 603 (1960).
[27] H. E. Radford, V. W. Hughes, and V. Beltran-Lopez, Bull. Am. Phys. Soc. **5**, 272 (1960); Phys. Rev. **123**, 153 (1961).
[28] H. Wieder, thesis, Case Institute of Technology, 1964 (unpublished).
[29] K. C. Brog, T. G. Eck, and H. Wieder, Phys. Rev. **153**, 91 (1967).
[30] In Ref. 6 a value of 4.7 a.u. was taken from Ref. 12 for the internuclear distance of the F_2^- molecule. The numbers in Table II have been recalculated using the better value of 4.0 a.u. (Ref. 12, private communication). Because of the crude nature of the calculations the results are qualitatively the same. For a discussion of the effects of lattice distortion on these contact values and of the effects of exchange polarization on the dipole-dipole hyperfine constants see Refs. 20(b) and 20(c).

is constructed from $2p$ atomic orbits neglecting overlap normalization. The radial part of $\psi(2p)$ is taken as that of the F^- ion.[31] The amount of polarization of $\psi(2p)$ at a given nuclear site is taken as *one-half* the polarization of the *fluorine atom at the same value of* $\psi(2p)$, as predicted by the unrestricted Hartree-Fock calculation.[24] Then the values of Gourary and Adrian[32] for orthogonalizing a plane wave to the closed ion shells are used. The internuclear distance for the F_2^- molecule is taken as 4.0 a.u. from the theoretical work of Das, Jette, and Knox.[12] Relaxations of the lattice nuclei were neglected. Column 3 of Table II gives the positive contact interaction due to σ_u if exchange polarization is neglected. Column 4 gives the predicted a_c values with exchange polarization. In addition to giving a correct order of magnitude for the negative a_c values of the A, B, C, and D nuclei, reduced a_c values are predicted for the E and F nuclei which are in favorable positions for large overlaps with σ_u. Experimentally the a_c value for the E nuclei is near zero due to a cancellation of positive and negative contributions. An improvement on the crude assumptions used in this calculation would require a detailed treatment of each of the points discussed above; nevertheless, the polarization of the closed shell molecular orbits seems to be the physical origin of the observed a_c values.

These negative contact interactions correspond to polarizations of the closed shell molecular orbitals at the nuclear sites of 10–30%. The actual numbers are not listed since they have little meaning (but they do indicate the large polarizations necessary to give approximate agreement with experiment). These values are much larger than the polarization of $|\psi(0)|^2$ that is usually observed at the nucleus of a magnetic ion. Indeed, the unrestricted Hartree-Fock[24] calculations predict a sign reversal in the net spin density of the fluorine atom at large values of radius. It is believed that the a_c values determined in this experiment indicate that such large polarizations at large distances do occur.

One important assumption made on the many electron aspects of this problem is that the exchange polarization of the molecular orbitals can be treated separately from the orthogonalization of the molecular electrons to the lattice ion electrons. Since we are considering regions of low electron density, this assumption seems reasonable. However, no attempt has been made to justify it outside of the comparison with the experimental results.

The polarization of the closed shell molecular orbitals appears to be more important than the overlap polarization of the lattice ions by an order of magnitude. Therefore, one would expect similar behavior in other systems where closed electron shells have about the same radial dependence as the unpaired spins. For example, lattice nuclei on nodal planes of a d^9 system would have negative contact interactions due to polarization of the closed shell d orbitals. On the other hand, lattice nuclei on nodal planes of a d^1 system would have smaller contact interactions due to the overlap polarization of the ion electrons. The situation may be more complicated for $4f$ electrons of rare-earth ions because the overlap with the lattice ions would come from the $5s$ and $5p$ closed shells.[23] In this case the lattice nuclei in the direction of an f lobe may have negative contact interactions.

V. CONCLUSION

The results of this ENDOR study of the V_K center may be explained by the self-trapped hole model that has previously been used to explain the results of ESR and optical studies. The variations in the ENDOR spectra taken for different ESR lines are explained by detailed consideration of the entire Hamiltonian including hyperfine interactions of the electron with both the lattice nuclei and the two molecular nuclei. Most of the ENDOR nuclei have negative contact hyperfine interactions, which seems to be explained by exchange polarizations of the closed shell molecular orbitals by the unpaired σ_u electron.

[31] C. Froese, Proc. Cambridge Phil. Soc. **53**, 206 (1957).
[32] B. S. Gourary and F. J. Adrian, Solid State Phys. **10**, 127 (1956).